nature neuroscience

Basal forebrain circuit for sleep-wake control

Min Xu[1,4], Shinjae Chung[1,4], Siyu Zhang[1], Peng Zhong[1], Chenyan Ma[1], Wei-Cheng Chang[1], Brandon Weissbourd[2], Noriaki Sakai[3], Liqun Luo[2], Seiji Nishino[3] & Yang Dan[1]

The mammalian basal forebrain (BF) has important roles in controlling sleep and wakefulness, but the underlying neural circuit remains poorly understood. We examined the BF circuit by recording and optogenetically perturbing the activity of four genetically defined cell types across sleep-wake cycles and by comprehensively mapping their synaptic connections. Recordings from channelrhodopsin-2 (ChR2)-tagged neurons revealed that three BF cell types, cholinergic, glutamatergic and parvalbumin-positive (PV+) GABAergic neurons, were more active during wakefulness and rapid eye movement (REM) sleep (wake/REM active) than during non-REM (NREM) sleep, and activation of each cell type rapidly induced wakefulness. By contrast, activation of somatostatin-positive (SOM+) GABAergic neurons promoted NREM sleep, although only some of them were NREM active. Synaptically, the wake-promoting neurons were organized hierarchically by glutamatergic→cholinergic→PV+ neuron excitatory connections, and they all received inhibition from SOM+ neurons. Together, these findings reveal the basic organization of the BF circuit for sleep-wake control.

The sleep-wake cycle is a fundamental biological process observed throughout the animal kingdom[1], and its disruption causes a variety of detrimental effects. Following the landmark studies by Von Economo[2] and Nauta[3], multiple brain regions have been identified as being involved in sleep-wake control, including the brainstem, hypothalamus and BF[4–7]. The neuronal activity in these regions changes between brain states[8–14], and their roles in sleep-wake regulation have been demonstrated using lesion, electrical stimulation and pharmacological manipulations[2,3,7,8,15–23]. In particular, lesion or inactivation of the BF was found to increase delta electroencephalogram (EEG) activity and decrease behavioral arousal in some studies[16,20,21], but reduced sleep in others[8,15,18]. These studies suggest that the BF is crucial for both sleep and wakefulness, but it is unclear which BF neurons promote each brain state and how they interact with each other.

There are three major neuronal types in the BF: cholinergic, glutamatergic and GABAergic. The cholinergic neurons are known to be active during both wakefulness and REM sleep, but are silent during NREM sleep[24], and their activation enhances arousal, attention and memory[23,25–29]. The glutamatergic and GABAergic neurons are also likely to have key roles in sleep-wake control[21]. However, their functional properties are much less understood. Furthermore, anatomical studies have shown that both cholinergic and non-cholinergic neurons make extensive synaptic contacts in the BF[30], but little is known about the rules of connectivity between the cell types and how they contribute to sleep-wake control. We used optogenetic methods to characterize the functional properties of individual BF cell types *in vivo* and to map their synaptic connections in brain slices, thus providing, to the best of our knowledge, the first comprehensive BF circuit diagram for sleep-wake control.

RESULTS

Genetically defined cell types

To target different cell types for recording and optogenetic activation, we used choline acetyltransferase (ChAT)-Cre, vesicular glutamate transporter 2 (VGLUT2)-Cre, PV-Cre and SOM-Cre mice for cell type–specific expression of fluorescent proteins and ChR2. These mouse lines were chosen because ChAT is a reliable, widely used marker for cholinergic neurons, and, of VGLUT1–3 (specific markers for glutamatergic neurons), VGLUT2 is the predominant marker in the BF[31] (*in situ* hybridization data are available in Allen Mouse Brain Atlas, Allen Institute for Brain Science: http://mouse.brain-map.org/experiment/show/70436317, http://mouse.brain-map.org/experiment/show/73818754 and http://mouse.brain-map.org/experiment/show/71587918 for VGLUT1, 2 and 3, respectively). The GABAergic neurons in the BF are known to be functionally diverse[13], and PV and SOM have been used as markers for different subtypes of GABAergic neurons in both the BF[11,30] and other brain regions[32].

To visualize these genetically defined cell types, we crossed each Cre driver mouse with a tdTomato reporter mouse (Ai14)[33]. Comparison of tdTomato expression with immunohistochemical staining or *in situ* hybridization of the four markers showed high specificity of labeling in each Cre line and low overlap between neurons expressing different markers (in most cases, the overlap was <1%, with the exception of PV+ neurons: ~5% of tdTomato-labeled neurons in PV-Cre mice also expressed VGLUT2, and ~10% immunohistochemically identified PV+ neurons were labeled by tdTomato in SOM-Cre mice; **Fig. 1** and **Supplementary Table 1**). Thus, ChAT+, VGLUT2+, PV+ and SOM+ neurons constitute largely distinct BF populations.

[1]Division of Neurobiology, Department of Molecular and Cell Biology, Helen Wills Neuroscience Institute, Howard Hughes Medical Institute, University of California, Berkeley, California, USA. [2]Department of Biology, Howard Hughes Medical Institute, Stanford University, Stanford, California, USA. [3]Sleep and Circadian Neurobiology Laboratory, Psychiatry and Behavioral Sciences, Stanford University School of Medicine, Palo Alto, California, USA. [4]These authors contributed equally to this work. Correspondence should be addressed to Y.D. (ydan@berkeley.edu).

Received 6 August; accepted 24 September; published online 12 October 2015; doi:10.1038/nn.4143

Sleep-wake activity of different cell types

To measure the firing rates of each cell type across natural sleep-wake cycles, we tagged the neurons with ChR2 by crossing the respective Cre driver mouse with a ChR2 reporter mouse (Ai32)[34] or by injecting Cre-inducible adeno-associated virus (AAV) expressing ChR2 into the BF of the Cre mouse. Recordings were made in freely moving mice using optrodes consisting of an optic fiber surrounded by several stereotrodes (**Fig. 2a**). High-frequency laser pulse trains (16 or 33 Hz, 5 ms per pulse; **Fig. 2b**) were applied intermittently, and single units exhibiting reliable laser-evoked spiking at short latencies were identified as ChAT+, VGLUT2+, PV+ or SOM+ neurons in the respective mouse line[35] (Online Methods and **Fig. 2c–f**).

We recorded from 85 identified neuron for 36–136 (median 105) min each, encompassing multiple cycles of wake, NREM and REM states classified by EEG and electromyogram (EMG) recordings (Online Methods and **Fig. 3a**). Cholinergic neurons typically fired a few spikes per second during wakefulness (3.9 ± 0.6 spikes per s, s.e.m.) and REM sleep (2.7 ± 0.4 spikes per s), but at much lower rates during NREM sleep (0.4 ± 0.1 spikes per s; **Supplementary Movie 1** and **Supplementary Fig. 1a**), consistent with previous studies using juxtacellular recording from head-fixed rats[24]. To quantify the relative firing rates of each neuron in different brain states, we plotted its REM-NREM modulation $((R_{REM} - R_{NREM})/(R_{REM} + R_{NREM})$, where R is the mean firing rate within each state) versus wake-NREM modulation $[(R_{wake} - R_{NREM})/(R_{wake} + R_{NREM})]$ (**Fig. 3b**). The gray shading indicates <2-fold firing rate change (|modulation| < 0.33), which was considered to be 'state indifferent' by previous investigators[8]. All of the identified cholinergic neurons (n = 12) fell into quadrant I (top right) outside of the gray shading, indicating that they were strongly modulated, wake/REM-active neurons.

We then measured the firing rates of non-cholinergic cell types, which have been less well characterized in previous studies. Of the 30 glutamatergic neurons identified in VGLUT2-ChR2 mice, the vast majority also fell into quadrant I (**Fig. 3c**,**d**). The few neurons found in other quadrants (4 of 30) were all in the gray-shaded area, indicating weak firing-rate modulation. Thus, glutamatergic BF neurons were also primarily wake/REM active. Unlike the ChAT+ neurons, however, many VGLUT2+ neurons were only weakly modulated across brain states (20 of 30 in gray-shaded area). The firing rates of the VGLUT2+ neurons (wake, 19.5 ± 3.2 spikes per s; NREM, 15.9 ± 3.0; REM, 19.8 ± 3.2, s.e.m.; **Supplementary Fig. 1b**) were also much higher than those of the cholinergic neurons ($P < 0.003$ for all three states, t test).

The PV+ GABAergic neurons exhibited even higher firing rates than glutamatergic neurons across all brain states (wake, 30.7 ± 4.3 spikes per s; NREM, 25.2 ± 4.2; REM, 33.9 ± 4.6, s.e.m., $P < 0.04$, t test; **Supplementary Fig. 1c**). Most of them were weakly modulated (**Fig. 3e**,**f**), with the majority found in quadrant I (wake/REM-active) and a few in quadrant II (REM active), consistent with a previous finding in anesthetized rats that PV+ neurons were more active during desynchronized EEG[11].

Recording from the SOM+ GABAergic neurons, we observed a number of strongly modulated NREM-active units (**Fig. 3g**,**h** and **Supplementary Fig. 1d**,**e**). Of the neurons not in the gray-shaded area (11 of 22), 5 of 11 strongly modulated neurons were highly active during NREM sleep (10 ± 6.4 spikes per s, s.e.m.) with low firing rates during wake (1.6 ± 1.3 spikes per s) and REM (3.8 ± 1.9 spikes per s) periods (**Supplementary Fig. 1d**). Such a firing pattern was not observed in any of the cholinergic, glutamatergic or PV+ GABAergic BF neurons.

Effects of BF neuron activation on sleep-wake states

We next tested the causal role of each cell type in sleep-wake control using ChR2-mediated activation. To ensure localized ChR2

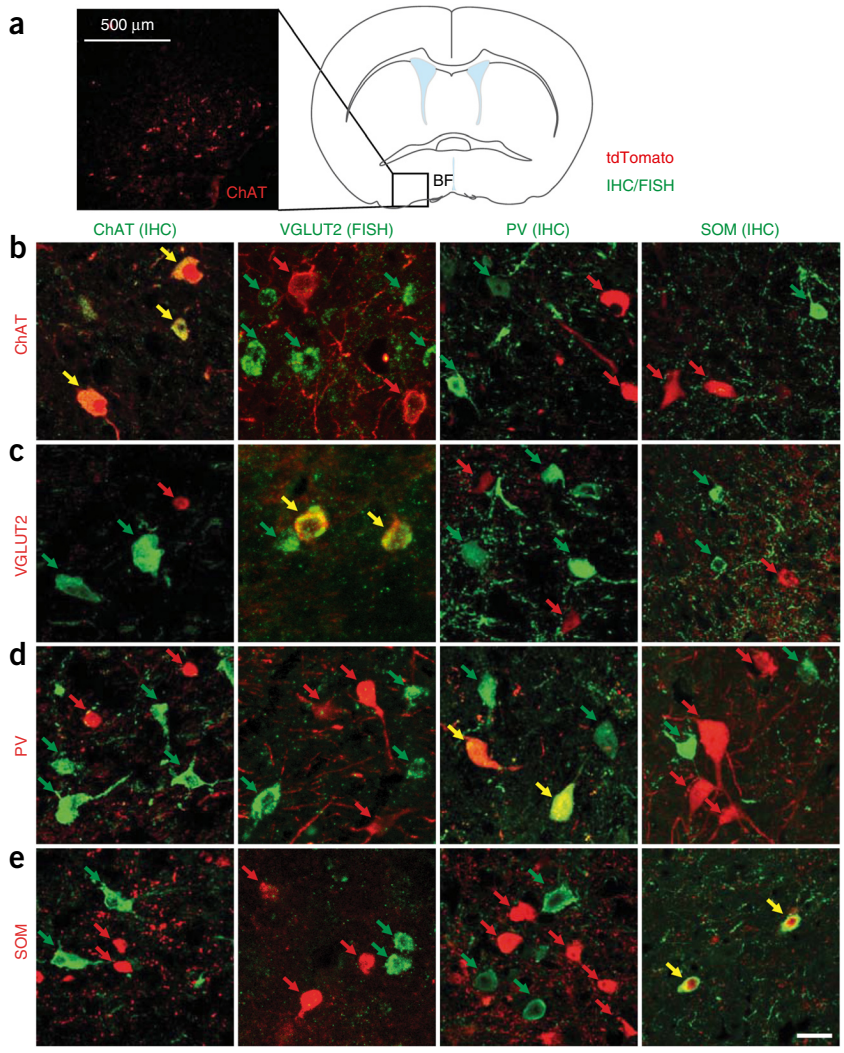

Figure 1 Genetically defined BF cell types. (**a**) Fluorescence image of BF (box in coronal diagram) showing tdTomato-expressing cholinergic neurons in ChAT-Cre × Ai14 mouse. (**b**) Fluorescence images of tdTomato (red) and immunohistochemical (IHC) staining or *in situ* hybridization for ChAT, VGLUT2, PV and SOM (green) in ChAT-Cre × Ai14 mouse. (**c**–**e**) Data presented as in **b**, but for VGLUT2-Cre (**c**), PV-Cre (**d**) and SOM-Cre (**e**) mice crossed with Ai14 mouse. Red, green and yellow arrows indicate cells that are tdTomato+, immunostaining/*in situ* hybridization+ and both, respectively. Scale bar represents 20 µm.

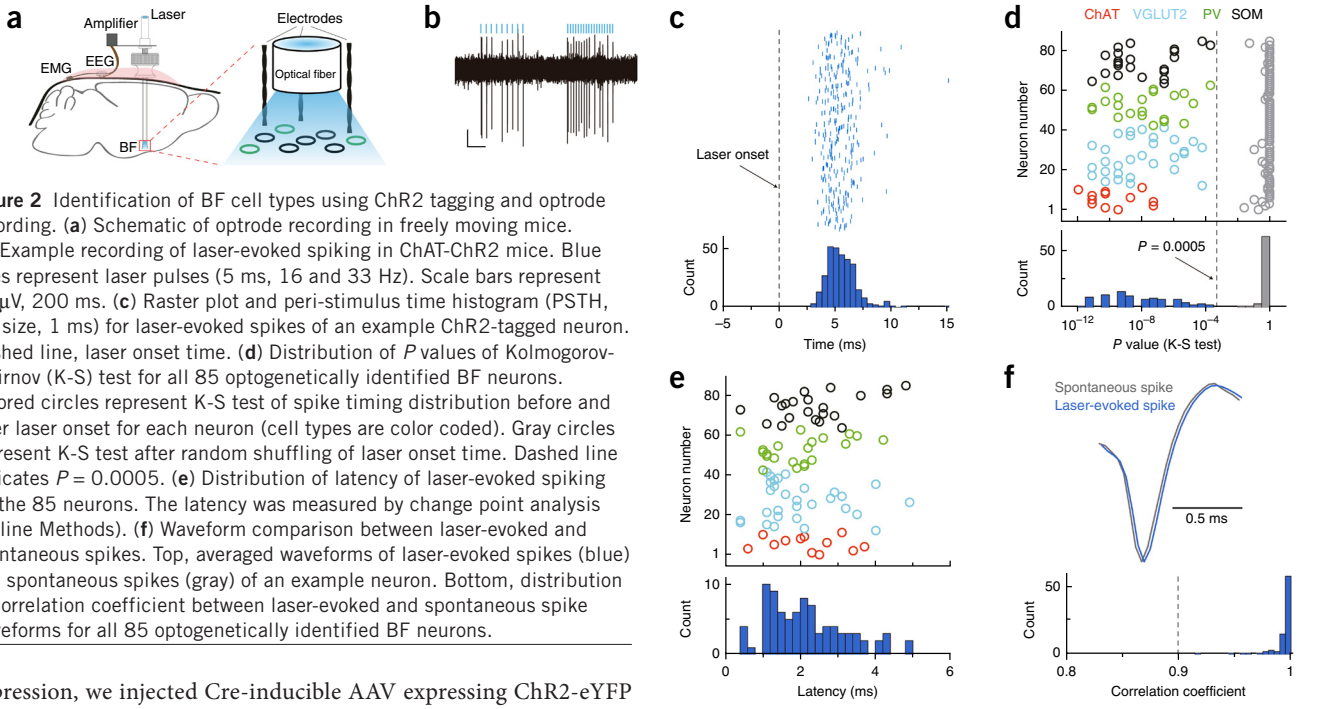

Figure 2 Identification of BF cell types using ChR2 tagging and optrode recording. (**a**) Schematic of optrode recording in freely moving mice. (**b**) Example recording of laser-evoked spiking in ChAT-ChR2 mice. Blue lines represent laser pulses (5 ms, 16 and 33 Hz). Scale bars represent 50 μV, 200 ms. (**c**) Raster plot and peri-stimulus time histogram (PSTH, bin size, 1 ms) for laser-evoked spikes of an example ChR2-tagged neuron. Dashed line, laser onset time. (**d**) Distribution of *P* values of Kolmogorov-Smirnov (K-S) test for all 85 optogenetically identified BF neurons. Colored circles represent K-S test of spike timing distribution before and after laser onset for each neuron (cell types are color coded). Gray circles represent K-S test after random shuffling of laser onset time. Dashed line indicates $P = 0.0005$. (**e**) Distribution of latency of laser-evoked spiking for the 85 neurons. The latency was measured by change point analysis (Online Methods). (**f**) Waveform comparison between laser-evoked and spontaneous spikes. Top, averaged waveforms of laser-evoked spikes (blue) and spontaneous spikes (gray) of an example neuron. Bottom, distribution of correlation coefficient between laser-evoked and spontaneous spike waveforms for all 85 optogenetically identified BF neurons.

expression, we injected Cre-inducible AAV expressing ChR2-eYFP into the BF of each Cre mouse (Online Methods and **Supplementary Fig. 2a**). We applied laser stimulation through optic fibers implanted bilaterally into the BF 3 weeks after injection (4–8 mW, 10 ms per pulse, 10 Hz, 60 s per trial; **Fig. 4a**).

We found that activation of cholinergic BF neurons induced a rapid desynchronization of the EEG and an increase in EMG power (**Fig. 4b**). Compared with the baseline period, laser stimulation caused a significant increase in wakefulness ($P = 1.6 \times 10^{-4}$, paired *t* test; **Fig. 4c**) and decrease in NREM sleep ($P = 4.8 \times 10^{-5}$), both by increasing the NREM→wake transition and by maintaining the wake state (**Supplementary Fig. 3a**). In control mice expressing eYFP without ChR2, laser stimulation had no effect ($P = 0.95$, 0.51 and 0.35 for wake, NREM and REM, respectively; **Fig. 4d**), and the laser-induced increase in wakefulness was significantly greater in ChR2 than

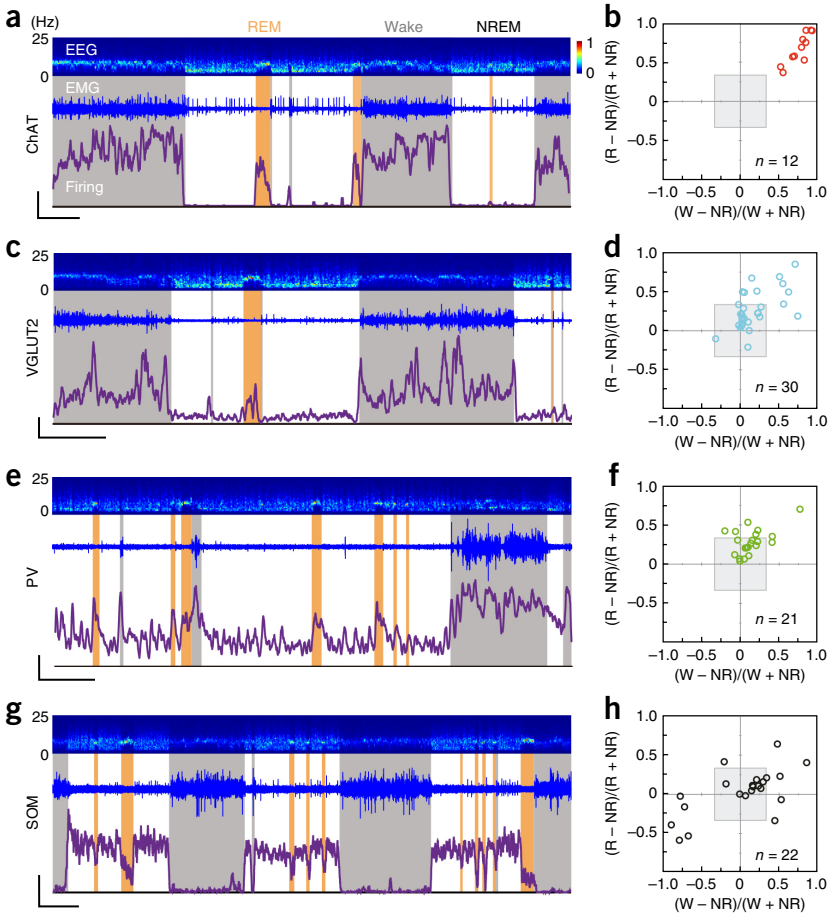

Figure 3 Firing rates of identified BF cell types across natural sleep-wake cycles. (**a**) Firing rates of an example ChAT+ neuron over 108 min. Top, EEG power spectrogram (0-25 Hz). Middle, EMG trace. Bottom, firing rate of the ChAT+ neuron. Scale bars represent 3 spikes per s, 500 s. Brain states are color coded: wake (W), gray; REM, orange (R); NREM, white (NR). (**b**) Summary of firing-rate modulation of 12 ChAT+ neurons (from six mice). Gray shading indicates <2-fold firing rate change between brain states. Note that in this two-dimensional plot, firing rates are compared explicitly between wake and NREM and between REM and NREM, but not between wake and REM states. Neurons that were maximally active during REM sleep are located in the upper left quadrant (quadrant II) and part of the upper right quadrant (quadrant I; closer to the vertical than horizontal axis). (**c**,**d**), Data presented as in **a** and **b** for VGLUT2+ neurons (six mice). (**e**,**f**) Data presented as in **a** and **b** for PV+ neurons (five mice). (**g**,**h**) Data presented as in **a** and **b** for SOM+ neurons (five mice). Scale bars (**c**,**e**,**g**) represent 10 spikes per s, 500 s.

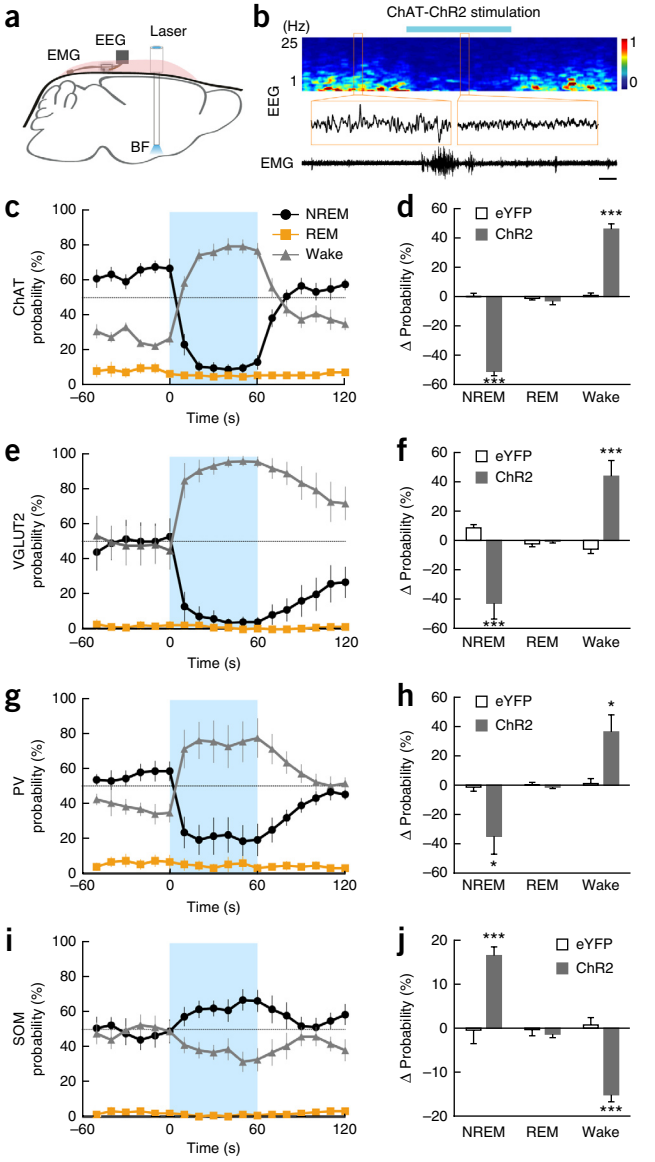

Figure 4 Effects of BF neuron activation on sleep-wake states. (**a**) Schematic of optogenetic stimulation experiment. (**b**) An example trial of ChAT+ neuron activation. Shown are EEG power spectrum, EEG traces during selected periods (indicated by boxes) and EMG trace during the whole trial. Blue bar represents period of laser stimulation (10-ms pulses, 10 Hz, 60 s). Scale bar represents 10 s. (**c**) Probability of wake, NREM or REM states before, during, and after laser stimulation of ChAT+ neurons ($n = 5$ mice). Error bars represent ±s.e.m. Blue shading indicates period of laser stimulation. (**d**) Laser-induced change in the probability of each state (difference between the 60-s periods before and during laser stimulation) in ChAT-ChR2 (filled bar) and ChAT-eYFP (open bar, $n = 3$) mice. Error bars represent ±s.e.m. (**e**,**f**) Data presented as in **c** and **d** for VGLUT2-ChR2 ($n = 6$) and VGLUT2-eYFP ($n = 5$) mice. (**g**,**h**) Data presented as in **c** and **d** for PV-ChR2 ($n = 6$) and PV-eYFP ($n = 4$) mice. (**i**,**j**) Data presented as in **c** and **d** for SOM-ChR2 ($n = 7$) and SOM-eYFP ($n = 4$) mice. The number of trials per mouse was 24–36. $^*P \leq 0.05$, $^{***}P \leq 0.001$ (difference between ChR2 and eYFP mice, two-way ANOVA followed by Bonferroni *post hoc* test).

in eYFP mice ($P = 6.4 \times 10^{-5}$, *t* test). Such a wake-promoting effect is consistent with previous findings based on cell type–specific lesion[20] or pharmacological manipulation[19].

For glutamatergic neurons, optogenetic activation also induced an immediate transition from NREM sleep to wakefulness ($P = 0.009$, paired *t* test; **Fig. 4e**,**f**, **Supplementary Movie 2** and **Supplementary Fig. 3b**). During laser stimulation, the probability of wakefulness approached 100%, attesting to the high efficiency of glutamatergic neurons in inducing wakefulness. Activation of PV+ GABAergic neurons also caused a significant increase in wakefulness ($P = 0.02$, paired *t* test) and decrease in NREM sleep ($P = 0.03$; **Fig. 4g**,**h** and **Supplementary Fig. 3c**), although the efficacy of these neurons appeared to be lower.

Activation of the SOM+ neurons, in contrast, caused a significant increase in NREM sleep ($P = 0.00014$, paired *t* test) and decrease in wakefulness ($P = 6 \times 10^{-5}$; **Fig. 4i**,**j** and **Supplementary Fig. 3d**). Thus, among the four BF cell types tested, SOM+ neurons were unique in their NREM-promoting effect, mirroring the finding that NREM-active neurons were only found in the SOM+ population (**Fig. 3h**).

Local connectivity among BF cell types

Ultrastructural studies have revealed numerous local synaptic contacts among BF neurons[30], which are likely to be important for sleep-wake regulation. We next mapped the local connectivity between the four BF cell types. ChR2 was expressed in the presynaptic cell type, and the postsynaptic cell type was either labeled with tdTomato or eGFP or identified using single cell reverse-transcription PCR (RT-PCR; **Fig. 5a** and Online Methods). For example, to test whether glutamatergic BF neurons innervate cholinergic neurons, we crossed the VGLUT2-Cre mouse with the ChAT-eGFP mouse and injected Cre-inducible AAV expressing ChR2-mCherry into the BF (see **Supplementary Table 2** for other pre- and postsynaptic pairs). We then made whole-cell recordings from the eGFP-labeled postsynaptic cells in acute BF slices while activating the ChR2-expressing presynaptic neurons with blue light (5 ms).

We detected extensive synaptic interactions among the BF cell types (**Fig. 5b**). Glutamatergic neurons excited cholinergic and both PV+ and SOM+ GABAergic neurons (**Fig. 5b**). Notably, cholinergic neurons excited PV+ neurons primarily through nicotinic acetylcholine (ACh) receptors (nAChRs), but provided strong inhibition to glutamatergic neurons through muscarinic AChRs (with very weak excitation; **Fig. 5c** and **Supplementary Fig. 4a**). Their innervations of SOM+ neurons were heterogeneous, consisting of excitatory and/or inhibitory inputs with a wide range of excitation/inhibition ratios (**Supplementary Fig. 4b**), likely related to the functional diversity of SOM+ neurons observed *in vivo* (**Fig. 3h**). PV+ neurons only weakly inhibited glutamatergic neurons, and no input was detected in cholinergic or SOM+ neurons (**Fig. 5d**), even though the light pulse activated PV+ neurons reliably, and spontaneous inhibitory currents were frequently observed in cholinergic neurons (**Supplementary Fig. 4c**). By contrast, SOM+ neurons provided strong $GABA_A$-mediated inhibition to glutamatergic, cholinergic and PV+ neurons (**Fig. 5e**).

Based on the functional characterization of each BF cell type (**Figs. 3** and **4**) and our connectivity mapping experiments (**Fig. 5**), we constructed a simple circuit diagram (**Fig. 5f**). The three wake-promoting cell types are organized in a hierarchical chain of excitatory connections (glutamatergic→cholinergic→PV+ neurons), with the feedback connections being either absent (PV+→cholinergic) or primarily inhibitory (cholinergic→glutamatergic, PV+→glutamatergic). Notably, the sleep-promoting SOM+ neuron population (dark circle) provides inhibition to all three wake-promoting cell types.

DISCUSSION

The BF is known to be important for both sleep and wakefulness[8,15,16,18,20,21], and it contains spatially intermingled wake- and

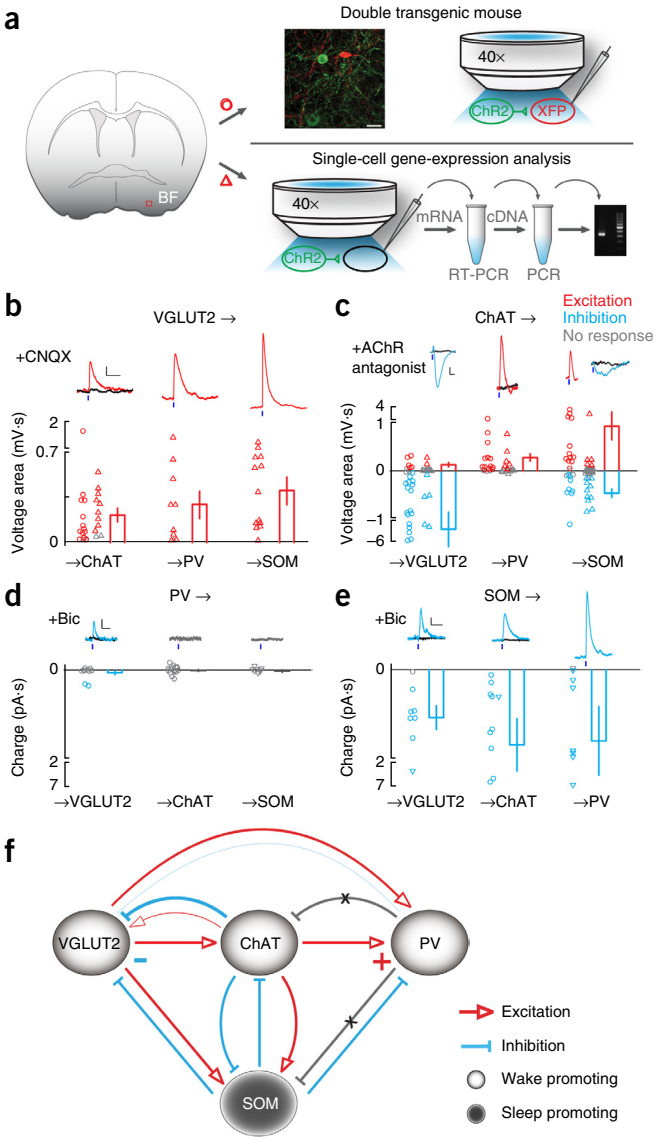

Figure 5 Local connectivity of BF cell types. (**a**) Schematic of slice experiment using two strategies. The first strategy (upper right) is to use double transgenic mice. Shown is a fluorescence image of a small BF area (red box in coronal diagram) showing ChR2-eYFP–expressing ChAT+ neurons (green) and tdTomato-expressing PV+ neurons (red) in an example experiment. Scale bar represents 30 μm. Blue light was used to activate ChR2-expressing (presynaptic) neurons and whole-cell recordings were made from fluorescently labeled postsynaptic neurons. The second strategy (lower right) requires single-cell gene-expression analysis. Recordings were made from unlabeled neurons and the cell type was identified using RT-PCR. (**b**–**e**) Synaptic interactions between multiple pairs of pre- and postsynaptic cell types. (**b**) VGLUT2+ to ChAT+, PV+ and SOM+ neuron connections. Top, example light-evoked excitatory responses (red) recorded under current clamp, blocked by the AMPA receptor antagonist CNQX (10 μM, black traces). Short blue bars indicate light pulses (5 ms). Scale bars represent 1 mV, 200 ms. Bottom, population summary of input strength (measured by voltage area, integral of excitatory postsynaptic potential); each circle (using double transgenic mice) or triangle (based on single-cell gene-expression analysis, performed in the presence of mAChR, nAChR antagonists) represents one cell. Red indicates significant excitatory response ($P < 0.05$, t test), gray indicates no significant response. Error bars represent ±s.e.m. (**c**) Data presented as in **b** for ChAT+ to VGLUT2+, PV+ and SOM+ connections (recorded under current clamp). Blue indicates significant inhibitory response ($P < 0.05$), black represents after application of AChR antagonists. ChAT→VGLUT2 excitatory response was blocked by nAChR antagonists MLA (methyllycaconitine, α7-containing nAChR antagonist, 5 nM) and DhβE (dihydro-β-erythroidine, non-α7 nAChR antagonist, 500 nM), and the inhibitory response was blocked by mAChR antagonist scopolamine (20 μM). ChAT→PV response was blocked by MLA + DhβE. ChAT→SOM excitatory responses were blocked by MLA, DhβE and scopolamine, and inhibitory responses were blocked by scopolamine. Scale bars represent 1 mV, 200 ms. All experiments indicated by triangle were performed in the presence of glutamate and GABA receptor antagonists. (**d**) PV+ to VGLUT2+, ChAT+ and SOM+ connections (voltage clamp). Of all of the recorded neurons (VGLUT2+, $n = 11$; ChAT+, $n = 17$; SOM+, $n = 8$), inhibitory responses were detected only in two VGLUT2+ neurons, which were blocked by $GABA_A$ receptor antagonist bicuculline (Bic, 20 μM, black trace). Scale bars represent 10 pA, 50 ms. (**e**) SOM+ to VGLUT2+, ChAT+ and PV+ connections (voltage clamp). All inhibitory responses (blue) were blocked by bicuculline (black). Scale bars represent 10 pA, 50 ms. (**f**) Diagram of BF local circuit. Light circles represent wake-promoting neurons. Dark circle represents sleep-promoting SOM+ neurons (containing both wake/REM-active and NREM-active neurons). Excitatory and inhibitory connections are indicated by red and blue lines, respectively. Gray lines with cross indicate tested connection with no detectable response. Connection strength is represented qualitatively by line thickness.

sleep-active neurons[8–10,12–14,36]. By recording and manipulating the activity of ChR2-expressing neurons in various Cre mice, we demonstrated the functional distinction between genetically defined cell types, especially for non-cholinergic neurons. This is a key step in dissecting the BF circuit for sleep-wake control.

Our circuit-mapping experiments suggest that the wake/REM-active property of cholinergic and PV+ neurons partly originates from the local glutamatergic input (**Fig. 5b**). Compared with the cholinergic neurons with well-characterized functions in wakefulness and arousal[16,23,25,27–29], we found that BF glutamatergic neurons showed an even stronger wake-promoting effect (**Fig. 4e** and **Supplementary Movie 2**). In addition to the larger number of light-activated VGLUT2+ neurons than ChAT+ and PV+ neurons (**Supplementary Fig. 2b**), this strong effect is also consistent with the BF circuit diagram (**Fig. 5f**): optogenetic activation of the glutamatergic neurons was able to excite both cholinergic and PV+ GABAergic neurons, each of which promoted wakefulness (**Fig. 4c**–**h**). In fact, the relative efficacy of glutamatergic, cholinergic and PV+ GABAergic neurons in inducing wakefulness is consistent with their positions in the hierarchical chain of excitation (**Fig. 5f**).

Notably, although optogenetic activation of BF cholinergic neurons caused a significant increase in wakefulness, we found no significant change in REM sleep ($P = 0.28$, paired t test; **Fig. 4d**). This finding is similar to that of a recent study[37], but different from another study using optogenetic activation[38]. In addition to differences in the stimulation protocol, there may be differences in the brain-state classification criteria. In our experiment, although laser stimulation in some trials induced EEG desynchronization without EMG change (**Supplementary Fig. 5b**), the EEG power spectrum in these trials was different from that in natural REM sleep (**Supplementary Fig. 5c**); thus, the brain state was left unclassified in our analysis (**Supplementary Fig. 5d**).

We found that activation of PV+ neurons in the BF evoked no detectable response in cholinergic or SOM+ neurons and only weak responses in glutamatergic neurons (**Fig. 5d**), which may be partly related to the relatively small number of PV+ neurons in the BF. On the other hand, their activation *in vivo* caused a significant increase in wakefulness, which may be mediated by long-range projections to outside of the BF. For example, in the cortex, axons of BF PV+ neurons have been shown to innervate GABAergic interneurons[39]

and may therefore disinhibit pyramidal neurons. In a recent study, optogenetic stimulation of BF PV+ neurons was also found to enhance gamma oscillations in the cortex[40]. Although we did not observe any prominent, specific increase in gamma band oscillation in the EEG, the difference may be a result of the different experimental protocols used in the two studies (for example, as the focus of our study was not on gamma oscillation, we did not use 40-Hz stimulation to test whether it is more effective than other frequencies in entraining cortical oscillations). In addition to the PV+ neurons, other BF cell types also send extensive long-range projections[41]. For example, cholinergic transmission in the cortex by BF ChAT+ neurons can cause rapid EEG desynchronization and enhanced behavioral performance[27–29,42].

Compared with the wake-promoting network, the circuits promoting sleep are much less understood[5]. Sleep-active neurons have been observed in the BF and several subregions of the hypothalamus[43]. In particular, the ventrolateral preoptic area (VLPO) has been shown to be a key region promoting NREM sleep, as cFos staining and electrophysiological recording have revealed a high density of sleep-active neurons in VLPO[44,45], and lesion of VLPO significantly reduces NREM sleep[46]. We found that optogenetic activation of BF SOM+ neurons rapidly increased the probability of NREM sleep (**Fig. 4i,j**), and some of these neurons were strongly NREM active (**Fig. 3g,h**). Whereas the GABAergic neurons in VLPO inhibit the monoaminergic neurons in the ascending arousal pathway[47,48], SOM+ neurons in the BF inhibit all three types of wake-promoting neurons (**Fig. 5e**). Thus, our results reveal a previously unknown pathway that promotes NREM sleep via broad inhibition of multiple wake-promoting cell types in the BF local circuit. Given the functional diversity of SOM+ neurons, it will be important for future studies to further divide them into different subgroups using additional molecular markers. In addition, as more effective optogenetic tools for neuronal silencing are developed, it would be important to test the effect of inactivating each cell type on brain states.

Complete understanding of sleep-wake control mechanisms requires elucidation of the functional roles of different cell types in relevant brain regions as well as the synaptic connections between them. Our findings illustrate the power of combining optogenetic manipulation with *in vivo* and *in vitro* electrophysiology in mapping the activity, causality and synaptic connectivity of specific cell types in sleep-wake control.

METHODS

Methods and any associated references are available in the online version of the paper.

Note: Any Supplementary Information and Source Data files are available in the online version of the paper.

ACKNOWLEDGMENTS

We thank J. Cox, F. Weber and N. Hirai for the help with data analysis, K. Kao for technical assistance, T. Hnasko (University of California, San Diego) for sharing VGLUT2-eGFP mice, and the Stanford Neuroscience Gene Vector and Virus Core for AAV-DJ.

AUTHOR CONTRIBUTIONS

M.X., S.C. and Y.D. conceived and designed the experiments. M.X. performed all of the optrode recording experiments, some of the *in situ* hybridization experiments and some of the slice recording experiments. S.C. performed histological characterization of BF cell types and all of the optogenetic activation experiments. S.Z. performed some of the slice experiments. P.Z. performed some of the slice recording experiments. C.M. and W.-C.C. performed some of the *in situ* hybridization experiments. N.S. and S.N. helped to establish sleep recording and data analysis. B.W. and L.L. provided reagents and helped to establish *in situ* hybridization. M.X., S.C. and Y.D. wrote the manuscript, and all of the authors helped with the revision of the manuscript.

COMPETING FINANCIAL INTERESTS

The authors declare no competing financial interests.

1. Siegel, J.M. Sleep viewed as a state of adaptive inactivity. *Nat. Rev. Neurosci.* **10**, 747–753 (2009).
2. Von Economo, C. Sleep as a problem of localization. *J. Nerv. Ment. Dis.* **71**, 249–259 (1930).
3. Nauta, W.J. Hypothalamic regulation of sleep in rats; an experimental study. *J. Neurophysiol.* **9**, 285–316 (1946).
4. Moruzzi, G. & Magoun, H.W. Brain stem reticular formation and activation of the EEG. *Electroencephalogr. Clin. Neurophysiol.* **1**, 455–473 (1949).
5. Saper, C.B., Fuller, P.M., Pedersen, N.P., Lu, J. & Scammell, T.E. Sleep state switching. *Neuron* **68**, 1023–1042 (2010).
6. Jones, B.E. Neurobiology of waking and sleeping. *Handb. Clin. Neurol.* **98**, 131–149 (2011).
7. Brown, R.E., Basheer, R., McKenna, J.T., Strecker, R.E. & McCarley, R.W. Control of sleep and wakefulness. *Physiol. Rev.* **92**, 1087–1187 (2012).
8. Szymusiak, R. & McGinty, D. Sleep suppression following kainic acid-induced lesions of the basal forebrain. *Exp. Neurol.* **94**, 598–614 (1986).
9. Szymusiak, R. & McGinty, D. Sleep-waking discharge of basal forebrain projection neurons in cats. *Brain Res. Bull.* **22**, 423–430 (1989).
10. Alam, M.N., McGinty, D. & Szymusiak, R. Thermosensitive neurons of the diagonal band in rats: relation to wakefulness and non-rapid eye movement sleep. *Brain Res.* **752**, 81–89 (1997).
11. Duque, A., Balatoni, B., Detari, L. & Zaborszky, L. EEG correlation of the discharge properties of identified neurons in the basal forebrain. *J. Neurophysiol.* **84**, 1627–1635 (2000).
12. Lee, M.G., Manns, I.D., Alonso, A. & Jones, B.E. Sleep-wake related discharge properties of basal forebrain neurons recorded with micropipettes in head-fixed rats. *J. Neurophysiol.* **92**, 1182–1198 (2004).
13. Hassani, O.K., Lee, M.G., Henny, P. & Jones, B.E. Discharge profiles of identified GABAergic in comparison to cholinergic and putative glutamatergic basal forebrain neurons across the sleep-wake cycle. *J. Neurosci.* **29**, 11828–11840 (2009).
14. Takahashi, K., Lin, J.S. & Sakai, K. Characterization and mapping of sleep-waking specific neurons in the basal forebrain and preoptic hypothalamus in mice. *Neuroscience* **161**, 269–292 (2009).
15. McGinty, D.J. & Sterman, M.B. Sleep suppression after basal forebrain lesions in the cat. *Science* **160**, 1253–1255 (1968).
16. Buzsaki, G. *et al.* Nucleus basalis and thalamic control of neocortical activity in the freely moving rat. *J. Neurosci.* **8**, 4007–4026 (1988).
17. Sallanon, M. *et al.* Long-lasting insomnia induced by preoptic neuron lesions and its transient reversal by muscimol injection into the posterior hypothalamus in the cat. *Neuroscience* **32**, 669–683 (1989).
18. Lin, J.S., Sakai, K., Vanni-Mercier, G. & Jouvet, M. A critical role of the posterior hypothalamus in the mechanisms of wakefulness determined by microinjection of muscimol in freely moving cats. *Brain Res.* **479**, 225–240 (1989).
19. Nishino, S. *et al.* Muscle atonia is triggered by cholinergic stimulation of the basal forebrain: implication for the pathophysiology of canine narcolepsy. *J. Neurosci.* **15**, 4806–4814 (1995).
20. Kaur, S., Junek, A., Black, M.A. & Semba, K. Effects of ibotenate and 192IgG-saporin lesions of the nucleus basalis magnocellularis/substantia innominata on spontaneous sleep and wake states and on recovery sleep after sleep deprivation in rats. *J. Neurosci.* **28**, 491–504 (2008).
21. Fuller, P.M., Sherman, D., Pedersen, N.P., Saper, C.B. & Lu, J. Reassessment of the structural basis of the ascending arousal system. *J. Comp. Neurol.* **519**, 933–956 (2011).
22. Deurveilher, S. & Semba, K. Basal forebrain regulation of cortical activity and sleep-wake states: Roles of cholinergic and non-cholinergic neurons. *Sleep Biol. Rhythms* **9**, 65–70 (2011).
23. Jones, B.E. The organization of central cholinergic systems and their functional importance in sleep-waking states. *Prog. Brain Res.* **98**, 61–71 (1993).
24. Lee, M.G., Hassani, O.K., Alonso, A. & Jones, B.E. Cholinergic basal forebrain neurons burst with theta during waking and paradoxical sleep. *J. Neurosci.* **25**, 4365–4369 (2005).
25. Everitt, B.J. & Robbins, T.W. Central cholinergic systems and cognition. *Annu. Rev. Psychol.* **48**, 649–684 (1997).
26. Sarter, M., Hasselmo, M.E., Bruno, J.P. & Givens, B. Unraveling the attentional functions of cortical cholinergic inputs: interactions between signal-driven and cognitive modulation of signal detection. *Brain Res. Brain Res. Rev.* **48**, 98–111 (2005).
27. Pinto, L. *et al.* Fast modulation of visual perception by basal forebrain cholinergic neurons. *Nat. Neurosci.* **16**, 1857–1863 (2013).
28. Fu, Y. *et al.* A cortical circuit for gain control by behavioral state. *Cell* **156**, 1139–1152 (2014).
29. Eggermann, E., Kremer, Y., Crochet, S. & Petersen, C.C. Cholinergic signals in mouse barrel cortex during active whisker sensing. *Cell Reports* **9**, 1654–1660 (2014).
30. Zaborszky, L. & Duque, A. Local synaptic connections of basal forebrain neurons. *Behav. Brain Res.* **115**, 143–158 (2000).

31. Lein, E.S. *et al.* Genome-wide atlas of gene expression in the adult mouse brain. *Nature* **445**, 168–176 (2007).
32. Xu, X., Roby, K.D. & Callaway, E.M. Immunochemical characterization of inhibitory mouse cortical neurons: three chemically distinct classes of inhibitory cells. *J. Comp. Neurol.* **518**, 389–404 (2010).
33. Madisen, L. *et al.* A robust and high-throughput Cre reporting and characterization system for the whole mouse brain. *Nat. Neurosci.* **13**, 133–140 (2010).
34. Madisen, L. *et al.* A toolbox of Cre-dependent optogenetic transgenic mice for light-induced activation and silencing. *Nat. Neurosci.* **15**, 793–802 (2012).
35. Anikeeva, P. *et al.* Optetrode: a multichannel readout for optogenetic control in freely moving mice. *Nat. Neurosci.* **15**, 163–170 (2012).
36. Modirrousta, M., Mainville, L. & Jones, B.E. Gabaergic neurons with alpha2-adrenergic receptors in basal forebrain and preoptic area express c-Fos during sleep. *Neuroscience* **129**, 803–810 (2004).
37. Irmak, S.O. & de Lecea, L. Basal forebrain cholinergic modulation of sleep transitions. *Sleep* **37**, 1941–1951 (2014).
38. Han, Y. *et al.* Selective activation of cholinergic basal forebrain neurons induces immediate sleep-wake transitions. *Curr. Biol.* **24**, 693–698 (2014).
39. Freund, T.F. & Meskenaite, V. Gamma-aminobutyric acid-containing basal forebrain neurons innervate inhibitory interneurons in the neocortex. *Proc. Natl. Acad. Sci. USA* **89**, 738–742 (1992).
40. Kim, T. *et al.* Cortically projecting basal forebrain parvalbumin neurons regulate cortical gamma band oscillations. *Proc. Natl. Acad. Sci. USA* **112**, 3535–3540 (2015).
41. Steriade, M. & McCarley, R.W. *Brain Control of Wakefulness and Sleep* (Plenum Press, New York, 2005).
42. Goard, M. & Dan, Y. Basal forebrain activation enhances cortical coding of natural scenes. *Nat. Neurosci.* **12**, 1444–1449 (2009).
43. Szymusiak, R., Gvilia, I. & McGinty, D. Hypothalamic control of sleep. *Sleep Med.* **8**, 291–301 (2007).
44. Sherin, J.E., Shiromani, P.J., McCarley, R.W. & Saper, C.B. Activation of ventrolateral preoptic neurons during sleep. *Science* **271**, 216–219 (1996).
45. Szymusiak, R., Alam, N., Steininger, T.L. & McGinty, D. Sleep-waking discharge patterns of ventrolateral preoptic/anterior hypothalamic neurons in rats. *Brain Res.* **803**, 178–188 (1998).
46. Lu, J., Greco, M.A., Shiromani, P. & Saper, C.B. Effect of lesions of the ventrolateral preoptic nucleus on NREM and REM sleep. *J. Neurosci.* **20**, 3830–3842 (2000).
47. Sherin, J.E., Elmquist, J.K., Torrealba, F. & Saper, C.B. Innervation of histaminergic tuberomammillary neurons by GABAergic and galaninergic neurons in the ventrolateral preoptic nucleus of the rat. *J. Neurosci.* **18**, 4705–4721 (1998).
48. Steininger, T.L., Gong, H., McGinty, D. & Szymusiak, R. Subregional organization of preoptic area/anterior hypothalamic projections to arousal-related monoaminergic cell groups. *J. Comp. Neurol.* **429**, 638–653 (2001).

ONLINE METHODS

Virus preparation. AAV2-EF1α-FLEX-ChR2-eYFP and AAV2-EF1α-FLEX-eYFP were produced by the University of North Carolina (UNC) Vector Core. The titer was estimated to be ~10^{12} genome copies (gc) ml^{-1}. AAV-DJ-EF1α-FLEX-ChR2-mCherry and AAV-DJ-EF1α-FLEX-eNpHR3.0-eYFP was produced by Neuroscience Gene Vector and Virus Core of Stanford University. The titer was estimated to be ~10^{13} gc ml^{-1}.

Animals. All experimental procedures were approved by the Animal Care and Use Committee at the University of California, Berkeley. *In vivo* optogenetic manipulation and recording experiments were performed on adult mice (include both genders, singly housed, naive before experiments, > P40, body weight 25–35 g). Slice recording were performed in young mice (>3 weeks).

The following mouse lines were used in the current study: mice from Jackson Laboratory (JAX# in parenthesis): ChAT-ChR2(H134R)-eYFP (014546); ChAT-IRES-Cre (006410); VGLUT2-IRES-Cre (016963); PV-IRES-Cre (008069); SOM-IRES-Cre (013044); ChAT-eGFP (007902); Ai14 tdTomato reporter (007914); Ai32 ChR2-eYFP reporter (012569); Mice from MMRRC: VGLUT2-eGFP (MMRRC#011835-UCD).

Surgery. To implant EEG and EMG recording electrodes, mice were anesthetized with 1.5–2% isoflurane (vol/vol). Two stainless steel screws were inserted into the skull 1.5 mm from midline and 1.5 mm anterior to the bregma, and two others were inserted 3 mm from midline and 3.5 mm posterior to the bregma. Two EMG electrodes were inserted into the neck musculature. Insulated leads from the EEG and EMG electrodes were soldered to a 2 × 3 pin header, which was secured to the skull using dental cement.

For all the experiments, we targeted the caudal portion of the BF (including the horizontal limb of the diagonal band of Broca, magnocellular preoptic nucleus, and substantia innominata) rather than the rostral nuclei (medial septum and the vertical limb of the diagonal band of Broca). For optogenetic activation experiments (**Fig. 4**), a craniotomy (~0.5 mm in diameter) was made 0.1 mm anterior to bregma and 1.2-1.5 mm from midline (in the same surgery as for EEG and EMG implant), and 1 µl AAV (0.5 µl per hemisphere) was injected bilaterally into the BF (5.2–5.4 mm from cortical surface). We then implanted optic fibers bilaterally into the BF. Dental cement was applied to cover the exposed skull completely and to secure the implants to the screws. After surgery, mice were allowed to recover for at least 2 weeks before experiments. For optrode recording experiments, a custom-made optrode (see below) was implanted unilaterally into the BF using similar procedure as described above.

Polysomnographic recordings and analysis. Animals were housed on a 12-h dark/12-h light cycle (light on between 7:00 and 19:00). All optogenetic manipulation experiments were performed between 11:00 and 15:00. Most of the optrode recording experiments were carried out between 9:00 and 19:00, but a few were performed till 23:00. EEG and EMG electrodes were connected to flexible recording cables via a mini-connector. The signals were recorded and amplified using AM-Systems amplifiers, filtered (0.1–1,000 Hz or 10–1,000 Hz for EEG and EMG recordings, respectively) and digitized at 600 Hz using LabView. Spectral analysis was carried out using fast Fourier transform (FFT) and NREM, REM and wake states were semi-automatically classified using a sleep analysis software (SleepSign for Animal, Kissei Comtec America) for each 10-s epoch (wake: desynchronized EEG and high EMG activity; NREM sleep: synchronized EEG with high power at 0.5–4 Hz and low EMG activity; REM sleep: desynchronized EEG with high power at theta frequencies (6–9 Hz) and low EMG activity).

Optogenetic manipulation. Since crossing the Ai32 reporter mouse with a given Cre mouse causes ChR2 expression in multiple brain regions containing the corresponding cell type, local laser stimulation in the BF may activate passing axons from non-BF neurons. To ensure localized ChR2 expression, we injected a Cre-inducible AAV expressing ChR2-eYFP into the BF of each Cre mouse for all the optogenetic activation experiments in **Figure 4**.

Two fiber optic cables (200-µm diameter; ThorLabs) were each attached through an FC/PC adaptors to a 473 nm blue laser diode (Shanghai Laser & Optics Century Co. Ltd.), and light pulses were controlled by a Master 8 pulse stimulator (A.M.P.I.) that provided synchronous inputs to both lasers. The two fiber optic cables were connected to bilaterally implanted optic fibers 2 h before each experiment. During experiments, laser pulses (10 ms per pulse, 10 Hz, 4–8 mW, 60 s) were applied every 5 min. Each experimental session lasted for 2–3 h.

Optrode recording. To tag genetically defined BF neurons with ChR2, we used the following strategies: (1) transgenic mice expressing ChR2 in a specific neuronal type (ChAT-ChR2-eYFP), (2) crossing a Cre driver line with a ChR2 reporter line (PV-Cre × Ai32, VGLUT2-Cre × Ai32, SOM-Cre × Ai32), or (3) injecting Cre-inducible AAV expressing ChR2 into a Cre mouse (VGLUT2-Cre, SOM-Cre). To identify ChR2-expressing neurons in the BF of freely moving mice, custom-made optrodes (consisting of a 200-µm optical fiber and six pairs of stereotrodes) were used. The stereotrodes were made by twisting together two 25-µm diameter FeNiCr wires (Stablohm 675, California Fine Wire), and the wires were cut with sharp scissors and electroplated with platinum (H2PtCl6, Sigma-Aldrich) to an impedance of ~300 kΩ with a custom-built MSP430 MCU-controlled multi-channel plating device. The optrode assembly was mounted on a light-weight driver to allow vertical movement the optrode assembly to search for light-responsive neurons. Cortical EEG and EMG (see above) were also recorded for brain state classification. All signals were acquired using TDT system-3 workstation (RA16 pre-amplifier + RX5 base processor) controlled by OpenEx software (TDT). Extracellular signals were filter at 0.3–8 kHz and sampled at 25 kHz for offline spike detection and sorting. EEG and EMG were filtered at 0–300 Hz and sampled at 1.5 kHz. Recording location and virus expression were verified after recording though standard histology procedures.

To identify ChR2+ neurons, high-frequency laser pulse trains (0.5-8 mW, 473 nm) were delivered intermittently. In the majority of recording sessions, each trial consisted of three components that were 500 ms apart: (1) 5 ms pulse train at 16 Hz for 500 ms; (2) 5-ms pulse train at 33 Hz for 500 ms; (3) 200-ms step pulse. The stimulation was applied every 45 s throughout the recording to monitor unit stability. To analyze the firing rates of each neuron during different brain states, spikes recorded 0 – 4 s from onset of laser stimulation were excluded. For each cell type, the laser power was optimized to identify light-responsive neurons without changing the brain state. However, in VGLUT2-ChR2 mice, laser power sufficient for activating the recorded units often promoted wakefulness. In such cases, laser pulse trains were applied every 10 s during a period separate from the recording session.

To identify neurons with ChR2-mediated responses, we performed the following three analyses.

Distribution of spike timing. To determine whether each laser pulse caused a significant change in spike timing, we computed the PSTH triggered on each laser pulse (0.5-ms bin, from 15 ms before to 15 ms after each pulse; **Fig. 2c**), and used K-S test to compare the spike timing distributions before and after the pulse. Laser-responsive neurons were identified at $P < 0.0005$ (**Fig. 2d**). To validate the statistical method used here, we performed the same procedure after random shuffling the timing of laser pulses and found that the P value was typically > 0.5 (**Fig. 2d**). Thus the units satisfying our statistical criterion showed highly significant laser-evoked responses.

Latency. To assess whether these units were driven directly through ChR2 or indirectly through synaptic inputs, we analyzed the spike latency relative to each laser pulse. We first identified the time of maximal firing rate (t_{max}) of the up-sampled PSTH (0.1-ms resolution, linearly interpolated from 0.5-ms bins). We then tested the difference between the firing rates in each 5-point sliding window (from laser onset to t_{max}) and that before laser onset (t test). The latency was measured by the change point (t_{chg}), defined as the point following the last point with $P > 0.01$ (in all cases, P was found to be < 0.01 for all the windows between t_{chg} and t_{max}). We found that the latencies of the identified neurons were typically ~2 ms (2.1 ± 1.1 ms, s.d.; **Fig. 2e**), indicating that they were directly driven.

Spike-waveform correlation. In principle, stringent single unit sorting procedure should ensure that the spontaneous and laser-evoked spikes originate from the same neuron. Nevertheless, we tested the waveform similarity between laser-evoke and spontaneous spikes for all identified neurons. We first identified the peak of PSTH after laser pulse, and fitted the peak with a Gaussian function to determine the mean (t_{mean}) and s.d. (σ). We then searched for spikes between $t_{mean} - \sigma$ and $t_{mean} + \sigma$ after each laser pulse as laser evoked spikes. The correlation coefficient was computed between the average waveforms of these laser-evoked spikes and the spontaneous spikes. The correlation coefficients of most of the identified neurons in this study were >0.97 (0.99 ± 0.01, s.d.; **Fig. 2f**).

The optrode recording experiments were performed over multiple circadian windows, because to obtain stable recordings electrodes were moved slowly to search for units, and stabilization of the recording could take up to several hours.

doi:10.1038/nn.4143

To test whether the sleep-wake related firing rate modulation differs significantly between different circadian times, we divided the neurons of each type into three groups according to the time of recording and performed two-way ANOVA analysis. We found that the circadian time did not significantly affect brain state modulation in any of the four cell types (ChAT: $P_{BS} = 1.0 \times 10^{-6}$, $P_{CT} = 0.60$, $P_{interaction} = 0.34$; VGLUT2+: $P_{BS} = 0.0027$, $P_{CT} = 0.73$, $P_{interaction} = 0.69$; PV+: $P_{BS} = 2.4 \times 10^{-5}$, $P_{CT} = 0.43$, $P_{interaction} = 0.50$; SOM+: $P_{BS} = 3.0 \times 10^{-4}$, $P_{CT} = 0.19$, $P_{interaction} = 0.14$; BS, brain state; CT, circadian time).

Slice recording. To map the local connectivity between the four genetically defined cell types in the BF, ChR2 was selectively expressed in presynaptic neurons and tdTomato or eGFP was expressed in postsynaptic neurons using crossed transgenic mice and virus (**Supplementary Table 2**).

Slice recordings were made at P23–30. When virus injection was needed, AAV-DJ-EF1α-FLEX-ChR2-mCherry (400-600 nl) was injected into the BF, and recording was made 1 week after injection. Slice preparation was according to procedures described previously[49]. Mouse was deeply anaesthetized with 5% isoflurane. After decapitation, the brain was dissected rapidly and placed in ice-cold oxygenated HEPES buffered artificial cerebrospinal fluid (ACSF; in mM: NaCl 92, KCl 2.5, NaH_2PO_4 1.2, $NaHCO_3$ 30, HEPES 20, glucose 25, sodium ascorbate 5, thiourea 2, sodium pyruvate 3, $MgSO_4$·7H2O 10, $CaCl_2$·$2H_2O$ 0.5 and NAC 12, at pH 7.4, adjusted with 10 M NaOH), and coronal sections of the BF were made with a vibratome (Leica). Slices (350 µm thick) were recovered in oxygenated NMDG-HEPES solution (in mM: NMDG 93, KCl 2.5, NaH_2PO_4 1.2, $NaHCO_3$ 30, HEPES 20, glucose 25, sodium ascorbate 5, thiourea 2, sodium pyruvate 3, $MgSO_4$·$7H_2O$ 10, $CaCl_2$·$2H_2O$ 0.5 and NAC 12, at pH 7.4, adjusted with HCl) at 32 °C for 10 min and then maintained in an incubation chamber with oxygenated standard ACSF (in mM: NaCl 125, KCl 3, $CaCl_2$ 2, $MgSO_4$ 2, NaH_2PO_4 1.25, sodium ascorbate 1.3, sodium pyruvate 0.6, $NaHCO_3$ 26, glucose 10 and NAC 10, at pH 7.4, adjusted by 10 M NaOH) at 25 °C for 1-4 h before recording. All chemicals were from Sigma.

Whole-cell recordings were made at 30 °C in oxygenated solution (in mM: NaCl 125, KCl 4, $CaCl_2$ 2, MgSO4 1, NaH_2PO_4 1.25, sodium ascorbate 1.3, sodium pyruvate 0.6, $NaHCO_3$ 26 and glucose 10, at pH 7.4). Excitatory and inhibitory postsynaptic potentials were recorded using a potassium-based internal solution (in mM: potassium gluconate 135, KCl 5, HEPES 10, EGTA 0.3, MgATP 4, Na_2GTP 0.3, and sodium phosphocreatine 10, at pH 7.3, adjusted with KOH, 290–300 mOsm). IPSCs were recorded using a cesium-based internal solution (in mM: $CsMeSO_4$ 125, CsCl 2, HEPES 10, EGTA 0.5, MgATP 4, Na_2GTP 0.3, sodium phosphocreatine 10, TEACl 5, QX-314 3.5, at pH 7.3, adjusted with CsOH, 290–300 mOsm) and isolated by clamping the membrane potential of the recorded neuron at the reversal potential of the excitatory synaptic currents. The resistance of patch pipette was 3–5 MΩ. The cells were excluded if the series resistance exceeded 40 MΩ or varied by more than 20% during the recording period. To activate ChR2, we used a mercury arc lamp (Olympus) coupled to the epifluorescence light path and bandpass filtered at 450–490 nm (Semrock), gated by an electromagnetic shutter (Uniblitz). Blue light pulse (5 ms) was delivered through a 40 × 0.8 NA water immersion lens (Olympus) at a power of 1–2 mW. Data were recorded with a Multiclamp 700B amplifier (Axon instruments) filtered at 0–2 kHz and digitized with a Digidata 1440A (Axon instruments) at 4 kHz. Recordings were analyzed using Clampfit (Axon instruments).

Single-cell RT-PCR. At the end of each recording, cytoplasm was aspirated into the patch pipette, expelled into a PCR tube as described previously[50]. The single cell RT-PCR protocol was designed to detect the presence of mRNAs coding for ChAT, VGLUT2, PV and SOM. First, reverse transcription and the first round of PCR amplification were performed with gene-specific multiplex primer (**Supplementary Table 2**) using the SuperScript III One-Step RT-PCR kit (12574-018, Invitrogen) according to the manufacturer's protocol. Second, nested PCR was carried out using AmpliTaq Gold 360 PCR kit (4398886, Invitrogen) with nested primers for each gene (**Supplementary Table 2**). All multiplex primers were designed to target two different exons to differentiate mRNAs from genomic DNA[51–53]. The final PCR products were sequenced and verified. Amplification products were visualized via electrophoresis using 2% agarose gel. During single cell RT-PCR procedures, care was taken to minimize RNA degradation and contamination.

Immunohistochemistry and *in situ* hybridization. For immunohistochemistry, mice were deeply anaesthetized with isoflurane and immediately perfused using 0.1M phosphate-buffered saline (PBS) followed by 4% paraformaldehyde (wt/vol) in PBS. The brains were removed, and post-fixed in the same fixative overnight at 4 °C. For cryoprotection, brains were stored in 30% sucrose (wt/vol) in PBS overnight. Brains were embedded and mounted with Tissue-Tek OCT compound (Sakura finetek) and 20-µm sections were cut using a cryostat (Leica). Brain slices were washed using PBS, permeabilized using PBST (0.3% Triton X-100 (vol/vol) in PBS) for 30 min and then incubated with blocking solution (2% normal goat serum or normal donkey serum (vol/vol) in the PBST) for 1 h followed by primary antibody incubation overnight at 4 °C using following antibodies: anti-ChAT antibody (AB144P, Millipore; 1:1000), anti-PV antibody (24428, Immunostar; 1:1,000), anti-SOM antibody (MAB354, Millipore; 1:200). The next day, slices were washed three times with PBS and then incubated with appropriate secondary antibody (A 11008, Alexa Fluor 488 Goat Anti-Rabbit IgG or A-11055, Alexa Fluor 488 Donkey Anti-goat IgG, Invitrogen; 1:500) for 2 h and coverslipped.

In situ hybridization for VGLUT2, GAD1 or GAD2 was performed as previously described[54,55]. Cryosections (50 µm thick) were collected into a 24-well plate, fixed in 4% paraformaldehyde, rinsed with PBS, and incubated with Proteinase K buffer. After fixing again with 4% paraformaldehyde and rinsing with PBS, the sections were incubated with acetylation buffer, washed with PBS, and then incubated with hybridization buffer (without the probe) for 1 h. Probes were added and sections were incubated at 50–65 °C for 16–20 h. After hybridization, sections were washed, first with 2 × SSC-50% formamide (vol/vol), then with 2 × SSC, and then treated with RNase buffer. After blocking with 5% normal goat serum, sections were incubated with AP-conjugated anti-DIG antibody (1093274, Roche Applied Science, 1:1000), and anti-DsRed (632496, Clontech, 1:500) or anti-GFP antibodies (GFP-1020, Aves Labs, 1:500) overnight at 4 °C. After washing, anti-DsRed or GFP antibodies were detected by Alexa Fluor 488 conjugated secondary antibodies (Invitrogen), and the DIG-labeled probe was detected by Fast Red TR/Naphthol AS-MX (F4523, Sigma-Aldrich). All probes were synthesized using published primers (Allen Institute for Brain Science, Allen Brain Atlas, http://www.brain-map.org), following the procedure described previously[54].

Fluorescence images were taken using a confocal microscope (LSM 710 AxioObserver Inverted 34-Channel Confocal, Zeiss) and Nanozoomer (Hamamatsu).

Statistics. *Samples size.* We did not perform a calculation on sample size. Our sample size is comparable to many studies using similar techniques and animal models.

Evaluation of brain states modulation upon optogenetic manipulations. All statistical tests were two-sided. Significant modulation by optogenetic manipulation for each cell type was assessed with a paired *t* test, *t* test or two-way repeated measures ANOVA with Bonferroni post-hoc comparisons. For *t* tests, data distributions were assumed to be normal, but this was not formally tested. Data collection and analysis were not performed blindly. Randomization was not performed, as majority of the experiments primarily involved within-animal comparisons.

Data exclusion criteria. Data from animals used in behavior experiments were excluded based on histological criteria that included injection sites, virus expression and optical fiber placement. Only animals with injection sites in the region of interest were included as shown in **Supplementary Figure 2**.

A **Supplementary Methods Checklist** is available.

49. Zhang, S. *et al.* Selective attention. Long-range and local circuits for top-down modulation of visual cortex processing. *Science* **345**, 660–665 (2014).
50. Lambolez, B., Audinat, E., Bochet, P., Crepel, F. & Rossier, J. AMPA receptor subunits expressed by single Purkinje cells. *Neuron* **9**, 247–258 (1992).
51. Pfeffer, C.K., Xue, M., He, M., Huang, Z.J. & Scanziani, M. Inhibition of inhibition in visual cortex: the logic of connections between molecularly distinct interneurons. *Nat. Neurosci.* **16**, 1068–1076 (2013).
52. Danik, M., Puma, C., Quirion, R. & Williams, S. Widely expressed transcripts for chemokine receptor CXCR1 in identified glutamatergic, gamma-aminobutyric acidergic, and cholinergic neurons and astrocytes of the rat brain: a single-cell reverse transcription-multiplex polymerase chain reaction study. *J. Neurosci. Res.* **74**, 286–295 (2003).
53. Nordenankar, K. *et al.* Increased hippocampal excitability and impaired spatial memory function in mice lacking VGLUT2 selectively in neurons defined by tyrosine hydroxylase promoter activity. *Brain Struct. Funct.* **220**, 2171–2190 (2015).
54. Weissbourd, B. *et al.* Presynaptic partners of dorsal raphe serotonergic and GABAergic neurons. *Neuron* **83**, 645–662 (2014).
55. Watakabe, A., Komatsu, Y., Ohsawa, S. & Yamamori, T. Fluorescent in situ hybridization technique for cell type identification and characterization in the central nervous system. *Methods* **52**, 367–374 (2010).